Development of 5- and 10-year-old pediatric phantoms based on polygon mesh surfaces

V.J. de Melo Lima
Department of Anatomy, Federal University of Pernambuco, Avenida Professor Moraes Rego 1235, CEP 50670-901, Recife, Pernambuco, Brazil

V.F. Cassola, R. Kramer [a)], C.A.B. de Oliveira Lira and H.J. Khoury
Department of Nuclear Energy, Federal University of Pernambuco, Avenida Professor Luiz Freire 1000, CEP 50740-540, Recife, Pernambuco, Brazil

J.W. Vieira
Federal Institute of Education, Science and Technology of Pernambuco, Avenida Professor Luiz Freire 500, CEP 50740-540, Recife, Pernambuco, Brazil, Polytechnic School of Pernambuco, University of Pernambuco, Rua Benfica 455, CEP 50751-460, Recife, Pernambuco, Brazil

Statement of provenance:
'This is an author-created, un-copyedited version of an article accepted for publication in Medical Physics. The American Association of Physicists in Medicine is not responsible for any errors or omissions in this version of the manuscript or any version derived from it. The definitive publisher authenticated version is available at DOI: 10.1118/1.3615623

Purpose
The purpose of this study is the development of reference pediatric phantoms for 5- and 10-year-old children to be used for the calculation of organ and tissue equivalent doses in radiation protection.

Methods
The study proposes a method for developing anatomically highly sophisticated pediatric phantoms without using medical images. The 5- and 10-year-old male and female phantoms presented here were developed using 3D modeling software applied to anatomical information taken from atlases and textbooks. The method uses polygon mesh surfaces to model body contours, the shape of organs as well as their positions and orientations in the human body. Organ and tissue masses comply with corresponding data given by the International Commission on Radiological Protection for the 5- and 10-year-old reference children. Bones were segmented into cortical bone, spongiosa, medullary marrow and cartilage to allow for the use of μCT images of trabecular bone for skeletal dosimetry.

Results
The four phantoms, a male and a female for each age, and their organs are presented in 3D images and their organ and tissue masses in tables which show the compliance of the ICRP reference values. Dosimetric data calculated for the reference pediatric phantoms by Monte Carlo methods were compared with corresponding data from adult mesh phantoms and pediatric stylized phantoms. The comparisons show reasonable agreement if the anatomical differences between the phantoms are properly taken into account.

Conclusions
Pediatric phantoms were developed without using medical images of patients or volunteers for the first time. The models are reference phantoms, suitable for the regulatory dosimetry, however, the 3D modeling method can also be applied to medical images to develop patient-specific phantoms.

I. INTRODUCTION

Children are more vulnerable to exposure from ionizing radiation than adults because most radiosensitive organs and tissues are anatomically still developing and additionally, they experience less shielding by overlying tissues in the pediatric body compared to the adult anatomy. Consequently, soon after the beginning of the adult phantom development in the sixties of the last century, pediatric phantoms began to emerge. Extending the mathematical or stylized adult MIRD5 phantoms, Cristy [1] and Cristy and Eckerman [2] from the Oak Ridge National Laboratory (ORNL) developed pediatric MIRD5 phantoms representing a newborn, a 1-, a 5-, a 10- and two 15-year-old children. Later, Han et al [3] revised the ORNL series of pediatric phantoms by including additional organs and updating the tissue compositions. The revised ORNL phantoms were used by Lee et al [4] to study the impact of the latest Recommendations of the International Commission on Radiological Protection (ICRP) [5] on the effective dose.

Contrary to the stylized phantoms, the development of voxel models began with the construction of pediatric phantoms. Pioneered by Williams et al [6] and Zankl et al [7], the whole body voxel phantoms BABY and CHILD were developed based on CT images of an 8-week-old newborn and of a 7-year-old child, respectively, and organ and tissue equivalent doses were calculated for X-ray procedures. Comprehensive studies on pediatric voxel phantoms were also carried out at the University of Florida (UF) for various ages. First, head and torso phantoms were developed which later received arms and legs [8, 9], as well as organ and tissue masses adjusted to corresponding data given by ICRP89 [10].

Hybrid computational models represent an important step in pediatric phantom development. Based on medical images acquired by CT or NMR from real bodies, this method then applies 3D modeling software to these images to create organs and body contours of unprecedented anatomical realism, better than in the voxel phantoms, but which can easily be changed, like in the stylized phantoms. Lee et al [11] from the UF were the first to present a hybrid phantom for the newborn and meanwhile a whole family of UF pediatric hybrid phantoms has followed [12, 13]. Based on whole body NMR images taken from volunteers, Christ et al [14] developed hybrid pediatric phantoms for a 5-year-old boy and an 11-year-old girl.

At the Department of Nuclear Energy at the Federal University of Pernambuco (DEN/UFPE), adult human phantoms have been developed over the last eight years [15, 16, 17]. The latest edition of the male and female adult, ICRP89-based, posture-specific phantoms, called MASH and FASH [18, 19, 20], have been developed from anatomical atlases and textbooks using 3D modeling software based on polygon mesh surfaces, i.e. without using medical images. The purpose of this study is to extend the phantom development program at DEN/UFPE to children by constructing male and female 5-year-old and 10-year-old mesh-based phantoms in standing posture using the same methods already applied to the development of the adult phantoms.

II. MATERIALS AND METHODS

In order to develop human phantoms without using medical images taken from patients or volunteers, one needs first, 3D objects of organs or 3D free-form objects, second, a detailed anatomical description of the human body, including all radiosensitive organs and tissues and third, computational tools to create and edit 3D objects with respect to volume, form, position and orientation. Most organs of the pediatric phantoms presented here were modeled using organs of the adult MASH and FASH phantoms [18, 19] as a starting point. Organs and tissues not represented in the adult phantoms were developed using 3D free-form objects based on polygon mesh surfaces and Bezier curves. The description of the human anatomy, especially for children, was found in textbooks and atlases [21-31], internet sites [32, 33] and cadaver specimens belonging to the Department of Anatomy at the UFPE. Specific information about the anatomy of the teeth was found in reference 29 and about

the distribution of cartilage in reference 24, for example. For most organs and tissues several sources were consulted, thereby providing complementary anatomical information.

The main computational tool used in this study was the 3D modeling software Blender 2.49b [34], a free, open source software for modeling, animating and other applications, such as the support for a variety of geometric primitives, including poly meshes, Bezier curves, NURBS surfaces and digital sculpting which allows for the creation, editing and voxelization of 3D objects. Additional software used were MakeHuman 0.9.1 RC1[35], a free, open source software for modeling of 3D humanoid characters based on a single and highly optimized mesh. The modeling is performed by deforming the mesh using an intuitive interface with the controls: age/sex, body mass, breast and body shape for the modeling of the body surface and ImageJ 1.43k [36] a free, open source Java-based image processing program for voxel volume adjustment developed by the National Institute of Health. Customized analysis and processing can be made by addition of Java-based plugins and/or macro language for the visualization and editing of voxelized phantoms. FANTOMAS [37], DIP [38] and QtVoxel [39] are special software packages also used for editing of the voxelized phantoms and for voxel number adjustment. The 5- and 10-year-old phantoms have organ and tissue masses based on reference data given by ICRP89 [10]. Tissue densities from ICRP89 [10] and from ICRU46 [40] were used to derive the corresponding target volumes for the modeling process. Finally, the pediatric phantoms were voxelized with a cubic resolution of 700 μm. A description of the modeling process is given below.

II.A. Body surface

The body surface of the 10-year-old phantom was developed using the parameter controls AGE/SEX, BODY MASS, BREAST, and SHAPE of the MakeHuman software. Figure 1 shows the MakeHuman interface with the parameter controls on the left and the humanoid body surface after modeling a 10-year-old child. Body proportions were adjusted based on data from Godin [21] and Snyder et al [23]. Using the same references [21, 23], the body surface for the 5-year-old phantom was derived as a down-scaled version of the 10-year-old surface because MakeHuman has a lower limit of 10 years for body surface modeling. The polygon mesh surfaces obtained with MakeHuman were then exported as wave front file to the Blender software for unification with skeletons and organs.

II.B. Skeleton

The body, especially the skeleton, of a child of 5 or 10 years of age has more resemblance with the male adult body, because of the larger pelvis of adult females which also affects the position of the lower long bones. Therefore first, the MASH skeleton was scaled down to fit into the 10-year old phantom surface imported from the MakeHuman software. Then the size and the position of the bones were changed according to anthropometric pediatric data for different body parts taken from Godwin [21] and Snyder et al [23]. After voxelization, the bones of the pediatric phantoms were segmented into cortical bone, medullary marrow, cartilage and spongiosa, which is trabecular bone filled with marrow, to allow for the use of μCT images of trabecular bone for skeletal dosimetry. The skeletal tissue volumes have been calculated similar to the method described earlier for the adult phantoms [41]. This method uses quantities taken or calculated from data found in ICRP publications to determine bone-specific tissue volumes. Age-specific skeletal tissue masses were taken from table 2.8 of ICRP89 [10] and are shown in table 1 together with their densities and the calculated tissue volumes. Red bone marrow mass fractions taken from table 9.4 in ICRP89 [10], cellularity factors taken from table 41 and bone mass fractions calculated from tables 8 and 9 in ICRP70 [42] are shown in table 2 together with mass ratios between cortical and trabecular bone for adults, taken from table 9.3 in ICRP89 [10], because pediatric data are currently not available for these quantities. The data presented in tables 1 and 2 were used to calculate the bone-specific volumes for cortical bone, spongiosa, medullary marrow and cartilage in the pediatric skeletons and will be shown in the result section. As

μCT images of trabecular bone for 5- and 10-year-old skeletons are currently not available, the μCT images used in the MASH and FASH phantoms for adults [43] were re-sampled to a 70 μm resolution, a method also used by Pafundi et al [50]. This procedure guarantees an integer ratio between the macro and the micro voxel resolutions of 700μm/70μm = 10, which is necessary for the insertion of the μCT images into the spongiosa macro voxels. The trabecular bone volume fractions (TBVFs) of the adult μCT images were adjusted to the percentages given by ICRP70 [42] for 5- and 10-year-old children. This is done with an algorithm which adds or subtracts trabecular bone surface micro voxels uniformly throughout the spongiosa volume until the targeted TBVF is achieved [51]. Table 3 shows the pediatric TBVFs together with those for adults. Similar to the adult skeletons, the images of the frontal bone were used for the cranium and the mandible, of the vertebra for the spine, of the sternum for the ribcage (ribs, clavicles, scapulae, sternum), of the iliac crest for the pelvis and of the femur for the long bones. The equivalent dose to the bone surface cells (BSC) was calculated for 50 μm thickness [44].

II.C. Organs and tissues

Forty-six organs and tissues have been modeled in each phantom, forty of which represent the organs and tissues listed in table 2.8 in ICRP89 [10], which contains the reference masses as a function of age. The target volumes for organs and tissues have been determined by dividing the ICRP89 reference masses by their corresponding densities. All other organ parameters, such as dimensions, shape and position in space or distances to neighboring organs have been taken from the anatomical data base quoted at the beginning of section II. Most organs and tissues were modeled using the 3D objects of the MASH and the FASH phantoms and changing them to pediatric dimensions by manipulating vertices and control points of the polygon mesh surfaces. As an example, figure 2 highlights one control point on the polygon mesh surface of the liver. Moving the control point in different directions also changes position and direction of the vertices which represent the connection between control points. Repeating this procedure with many control points allows for the modeling of the dimensions and the shape of the liver as well as its position in space.

Newly developed organs, such as ureters, uterine tubes, urethra, tonsils, pituitary gland, epididymes and blood vessels, were designed by applying techniques such as subdivision and extrusion to 3D free-form objects or Bezier curves [45]. Tubular structures, such as the small intestine, the colon and the ureters, were made using the editing tool "extrusion" of Bezier curves, a tool of the Blender software which allows modeling winding tubes with defined widths and wall thicknesses.

Lymphatic nodes located on both sides of the central sagittal plane were designed as ellipsoids using the DupliVert tool of the Blender software. DupliVert comes from *Dupli*cation at *Vert*ices and represents a method which duplicates all vertices of the polygon mesh of an object. Non-symmetrical lymphatic nodes were designed as spheres. The lymphatic nodes have been modeled in the mesh phantoms at the armpit, at the groins, behind the knees, in front of the elbows, at the neck, at the face, around large blood vessels of throat and trunk, as well as around abdominal soft-tissue organs. According to footnote c of table 2.8 in ICRP89 "separable connective tissue and certain lymphatic tissues account for most of the remaining 4% of body mass". Using this statement and table 11.2 on page 217 of ICRP89 on connective tissue masses, the masses of the lymphatic nodes were calculated as 60 g and 180 g for the 5- and 10-year-old, respectively.

Oral cavity, esophagus, stomach, small intestine and colon represent different parts of the digestive tube. Additionally, the digestive system contains the liver, the pancreas, the gall bladder and the salivary glands. Stomach, small intestine and colon were modeled as walled organs with content. The esophagus wall is represented by a closed tube, because without food or liquid being transported from the oral cavity to the stomach the esophagus contracts completely. The physiological lengths of the small intestines are 166 cm (170) and 211 (220) cm, and of the colon 74 cm (75) and 89 cm (90)

for the 5- and 10-year-old, respectively, with the reference values from ICRP89 shown in brackets, confirming good agreement.

II.D. Voxelization

The mesh phantoms had to be voxelized because the current version of the EGSnrc Monte Carlo (MC) code [46], mainly used at the DEN/UFPE for dosimetric purposes, can currently not be connected to 3D objects based on polygon mesh surfaces. Probably it is only a question of time until this becomes possible, but then one would have additionally to "mesh" the voxel-based μCT images of trabecular bone in order to continue using this type of skeletal dosimetry. The voxelization was done with the Blender software using cubic voxels of 700 μm, which, according to ICRP89 [10], is the total thickness of the skin for children less than 10 years of age. After voxelization, all surface voxels have the ID number for subcutaneous adipose tissue. The skin voxels were defined by re-tagging adipose surface voxels based on the following procedure: First, adipose voxels for which one of the 8 lateral neighbors is an air voxel are re-tagged as skin voxels. If the target volume for the skin was not achieved, which was the case for all mesh phantoms developed at DEN/UFPE until today, then the procedure is repeated with the 26 lateral and diagonal neighbors until the target volume is met. This procedure may produce small areas with skin thicknesses made of 2 or 3 voxels in some regions with curved surfaces, such as the chin, the cranium, the hands and the feet.

All organs and tissues have been modeled in the mesh phantoms, except for the skeletal tissues and the skin. The mesh phantoms were stored and are available in the future if new organs should be included or existing organs have to be revised. In the voxelized phantoms the volumes of all organs and tissues were fine-tuned to match the organ and tissue masses specified by ICRP89. Adult tissue compositions and densities [19] were used for the pediatric phantoms based on data taken from ICRP110 [44], except for bone and adipose tissue which were taken from ICRP89 [10] and ICRU46 [40] for the pediatric ages under consideration.

II.E. Dosimetry

The voxelized versions of the pediatric phantoms, F05, M05, F10 and M10, were connected to the EGSnrc Monte Carlo (MC) code [46], which is one of the best bench-marked MC codes for coupled photon/electron transport with a dynamic range of charged particle kinetic energies between a few tens of keV and a few hundred GeV, and of photon energies between 1 keV and several hundred GeV. Organ and tissue equivalent doses were calculated for the following exposure scenarios: External whole body exposure anterior-posterior (AP), posterior-anterior (PA) and rotational (ROT) with a parallel beam of photons and internal exposure to gamma emitters concentrated in selected organs. Cut-off energies were 2 keV for photons in all tissues, 20 keV for electrons in tissues outside the skeleton and 5 keV in skeletal tissues. Statistical errors were normally well below 1% or below 5% for incident photon energies below 20 keV. Organ and tissue equivalent doses for the pediatric phantoms will be compared with corresponding data for adult mesh-based phantoms and for pediatric MIRD5-type phantoms.

III. RESULTS AND DISCUSSION

III.A. The mesh phantoms

Anterior and lateral views of the 5- and 10-year-old reference mesh phantoms F05, M05 and F10, M10 are shown in figure 3. Adipose and muscle tissues have been made transparent to allow for the skeletons, internal organs and blood vessels to be seen. Male and female phantoms have the same body dimensions and organ masses, except for the primary sexual organs: testes, ovaries, epididymes, prostate, uterine tubes and uterus. Internal mesh organs and tissues are shown in figure 4 for the respiratory system, in figure 5 for the digestive system, in figure 6 for the circulatory and lymphatic systems and in figure 7 for the male urogenital system. Finally, remaining organs and tissues are shown in figure 8.

III.B. The voxelized phantoms

The pediatric mesh phantoms F05, M05, F10 and M10 were voxelized with a cubic resolution of 700 μm. Segmentation of skeletal tissue volumes and final adjustments of organ and tissue masses were done in the voxelized versions of the phantoms. Table 4 shows some of the important properties. For comparison, ICRP89 reference standing heights are 109 cm and 138 cm and total body masses are 19 kg and 32 kg for the 5- and 10-year-old child, respectively. Using the data shown in tables 1 and 2, the bone-specific skeletal tissue volumes for cortical bone, spongiosa, medullary marrow and cartilage have been calculated and segmented in the voxelized skeletons. They are shown in table 5 and 6 for the 5 and the 10-year-old skeletons, respectively.

Figure 9a shows a CT image from the chest region of a 9-year-old boy in supine posture and figure 9b the corresponding slice of the voxelized standing M10 phantom. Similar images are shown in figures 10a and 10b for the abdominal region.

The CT images are available at http://www.radiologyinfo.org/en/info.cfm?pg=pedia-ct, a website which provides radiological information to patients. A comparison between the CT images of this pediatric patient and the images of the M10 phantom has to take two facts into account: First, human anatomy as shown in textbooks and atlases represents an average individual, i.e. that differences with respect to organ shape and position of real humans are common. Second, it was shown that the posture of a person can make a difference with respect to the position of organs [19]. When a person changes his/her posture from standing to supine, abdominal organs are shifted in cranial and dorsal direction, especially the kidneys. This can be seen in the abdominal images where in figure 10a the kidneys are located closer to the dorsal part of the trunk compared to their position in figure 10a. In view of these circumstances, the comparison between the CT images 9a, 10a and the phantom images 9b, 10b is satisfactory.

Finally, segmented organ and tissue masses for all phantoms are shown in table 7 together with the ICRP89 reference masses. All important organ and tissue masses in the pediatric phantoms match the reference masses exactly, except for small differences for the skeletons: 0.4% for the 5-year-old and 0.8% for the 10-year-old phantom. Only the main blood vessels have been segmented in the pediatric phantoms. Therefore, blood mass appears explicitly as well as implicitly (included in other tissues) in table 7. Female brain and thymus masses are smaller than the male masses according to ICRP89 [10].

III.C. Dosimetric data

Figure 11 shows lateral views of the pediatric phantoms M05 and F10 together with the adult male and female mesh-based phantoms MASH3 and FASH3[19]. The differences of the anteroposterior

dimensions between the pediatric and the adult bodies suggest greater organ and tissue equivalent doses in the pediatric bodies for external exposure because of less shielding by overlying tissues and smaller organ masses.

Equivalent doses to the red bone marrow (RBM) and to the bone surface cells (BSC) per incident air kerma, calculated with the 8 SP cluster method [51], are shown in figure 12 for the pediatric M05 and the adult MASH phantoms. The Monte Carlo calculation simulated whole body exposure AP with photons. As expected, RBM and BSC equivalent doses in the MASH3 skeleton are smaller because the greater adult body mass provides more attenuation of the radiation before it reaches the bones compared to the male 5-year-old body. Additionally, the greater cellularity factors for the 5-year-old skeleton are also contributing to the increase of the RBM equivalent dose in the M05 phantom. Differences between equivalent doses in the M05 and the MASH3 skeleton averaged over the whole energy scale are factors of 2.2 and 2.3 for the RBM and the BSC, respectively. For energies below 20 keV these differences can reach more than a factor of 10.

Figure 13 shows similar quantities for the lungs and for the stomach wall of the F10 and the FASH3 phantoms. The differences between lungs and stomach wall equivalent doses for the two phantoms averaged over the entire energy scale are 25% for both organs. Differences up to a factor of 3 are possible for energies below 30 keV. These numbers are smaller than those seen before in figure 12 because F10 and FASH3 differ less than M05 and MASH3 with respect to body mass.

Effective doses ED_05, ED_10 and ED_ADULT are shown in figure 14 for the pediatric phantoms F05/M05, F10/M10 and the adult phantoms FASH/MASH for whole body exposure AP. ED_05 is greater than ED_10 on average by 5.7% between 10 keV and 10 MeV which is due to the greater body mass of the 10-year-old phantoms which causes more shielding for organs located below the adipose tissue layer. From this point of view, one would expect the adult effective dose to be smaller than both pediatric effective doses, but the contrary is the case: The adult effective dose ED_ADULT is on average by 9% greater than the average pediatric effective dose, mainly because of the dose to the glandular tissue of the breasts. Breasts, including glandular tissue, have not been segmented in the pediatric phantoms because table 2.8 in ICRP89 does not mention breast masses for children up to 10 years of age. In adults, glandular tissue, the radiosensitive part of the breasts, receives a high equivalent dose for AP exposure and has a high tissue weighting factor [5]. The product of these two quantities increases the adult effective dose significantly above the pediatric effective dose, for which this product is zero.

Specific absorbed fractions (SAFs) are shown in figure 15 for the F05, M10 and the MIRD5 phantoms of 5 and 10 years used in the OLINDA software [47]. For all cases, the SAFs for the MIRD5 phantoms are smaller than the F05 and the M10 SAFs because of the greater inter-organ distances in the MIRD5_type phantoms. For a given internal exposure scenario, the distance between the source and the target organ represents the most important exposure parameter. Smith et al [48] investigated the inter-organ distances in the GOLEM voxel phantom [49] and the adult MIRD5 phantom [2] and found differences by up to a factor of 3.

IV. CONCLUSIONS

Male and female polygon mesh surface phantoms for the ages of 5 and 10 years have been developed for the first time based only on anatomical atlases and textbooks using 3D modeling software and excluding the use of medical images from patients or volunteers. The method presented here allows for very detailed design of anatomical structures. The pediatric phantoms M05, F05, M10 and F10 have organ and tissue masses according to corresponding data given by ICR89 [10] for the reference 5- and 10-year-old and their positions are representative for children in standing posture. The models can be considered as ICRP-compliant voxel phantoms developed using mesh technique. Medical images

are usually taken from persons in supine posture which implies different organ positions [19], i.e. a phantom representing a standing child could not be made based on medical images. On the other hand, if the use of medical images is warranted, the method proposed here can also be used to model a supine patient-specific phantom.

Dosimetric data calculated with M05, F05, M10 and F10 are reasonable and satisfy the expectations when compared to the results for adult phantoms. The comparison with the stylized MIRD5 phantoms was reasonable if the anatomical differences between the two phantoms types were properly taken into account. The phantoms are the first of a series of pediatric reference phantoms which will be developed at the DEN/UFPE.

Mathematical, voxel, hybrid or just mesh, whatever method of development was applied, each phantom usually serves specific purposes which influence the properties of its anatomy. Reference phantoms, representing average individuals, have total body mass, standing height, organ and tissue masses in compliance with anatomical reference data given by ICRP89 [10]. They are mostly used for regulatory dosimetry in order to control effective or other dose limits or compare exposure levels at different radiological institutions, for example. Person- or patient-related phantoms have different postures, body masses, standing heights and organ masses. They can be used for patient dosimetry in X-ray diagnosis, for example. Organ and tissue equivalent doses for a patient with the same posture, body mass and standing height are similar to those determined with the corresponding patient-related phantom. However, they are only similar because organ positions can still be different between patient and phantom. Finally, patient-specific phantoms represent the closest match between a phantom and a real person, usually a patient to be submitted to radiotherapy. The use of medical images of the patient is absolutely necessary to model a true to nature 3D representation of the patient's body or of parts of it, including the exact volume, form and position of internal organs and tissues. In view of the mentioned categories of phantoms, the pediatric mesh models developed in this study based on anatomical atlases and textbooks represent reference phantoms to be used in regulatory dosimetry, i.e. that for patient-related dosimetry their use is limited and they should not be used for patient-specific dosimetry.

ACKNOWLEDGEMENTS

The authors would like to thank the Conselho Nacional de Desenvolvimento Científico e Tecnológico - CNPq and the Fundação de Amparo à Ciência do Estado de Pernambuco - FACEPE for financial support. Special thanks go to Prof. M. Stabin from Vanderbilt University for providing the OLINDA data.

a) Electronic mail: rkramer@uol.com.br

[1] M. Cristy, "Mathematical phantoms representing children of various ages for use in estimates of internal dose", Oak Ridge National Laboratory Report ORNL/NUREG/TM-367 (1980)
[2] M. Cristy and K. F. Eckerman, "Specific absorbed fractions of energy at various ages from internal photon sources", Oak Ridge National Laboratory Report ORNL/TM-8381/V1 (1987)
[3] E.Y. Han, W. E. Bolch and K. F. Eckerman, "Revisions to the ORNL series of adult and pediatric computational phantoms for use with the MIRD schema", Health Physics, **90**(4), 337-356 (2006)
[4] C. Lee, C. Lee, E.Y. Han and W. E. Bolch, "Considerations of the ICRP 2006 revised tissue weighting factors on age-dependent values of the effective dose for external photons", Phys. Med. Biol., **52**, 41-58 (2007)

[5]"Recommendations of the International Commission on Radiological Protection", ICRP Publication No. 103 (Pergamon, Oxford, 2007)
[6] G. Williams, M. Zankl, W. Abmayr, R.Veit and G. Drexler,"The calculation of dose from external exposures using reference and realistic human phantoms and Monte Carlo methods", Phys. Med. Biol., **31,** 449-452 (1986)
[7] M. Zankl, R. Veit, G. Williams, K. Schneider, H. Fendel, N. Petoussi and G. Drexler, "The construction of computer tomographic phantoms and their application in radiology and radiation protection", Radiat. Environ. Biophys., **27**, 153-164 (1988)
[8] C. Lee, J. L. Williams, C. Lee and W. E. Bolch,"The UF series of tomographic computational phantoms of pediatric patients", Med. Phys. **32**(12), 3537-3548 (2005)
[9] C. Lee, C. Lee, J. L. Williams and W. Bolch, "Whole-body voxel phantoms of pediatric patients – UF series B", Phys. Med. Biol. **51**, 4649-4661 (2006)
[10] "Basic Anatomical and Physiological Data for Use in Radiological Protection: Reference Values", ICRP Publication No. 89 (Pergamon, Oxford, 2002)
[11] C. Lee, D. Lodwick, D. Hasenauer, J. L. Williams, C. Lee and W. E. Bolch, "Hybrid computational phantoms of the male and female newborn patient: NURBS-based whole-body models", Phys. Med. Biol. **52** 3309-3333 (2007)
[12] C. Lee, D. Lodwick, J. L. Williams and W. E. Bolch, "Hybrid computational phantoms of the 15-year male and female adolescent: Application to CT organ dosimetry for patients of variable morphometry", Med. Phys. **35**(6), 2366-2382 (2008)
[13] C. Lee, D. Lodwick, J. Hurtado, D. Pafundi, J. L. Williams and W. E. Bolch, "The UF family of reference hybrid phantoms for computational radiation dosimetry", Phys. Med. Biol. **55**, 339-363 (2010)
[14] A. Christ, W. Kainz, E. G. Hahn, K. Honegger, M. Zefferer, E. Neufeld, W. Rascher, R. Janka, W. Bautz, J. Chen, B. Kiefer, P. Schmitt, H.-P. Hollenbach, J. Shen, M.Oberle, D. Szczerba, A. Kam, J. W. Guag and N. Kuster, "The virtual family – development of surface-based models of two adults and two children for dosimetric simulations", **55**, N23-N38 (2010)
[15] R. Kramer, J. W. Vieira, H. J. Khoury, F. R. A. Lima and D. Fuelle, "All About MAX: a Male Adult voXel Phantom for Monte Carlo Calculations in Radiation Protection Dosimetry", Phys. Med. Biol., **48**, 1239-1262 (2003)
[16] R. Kramer, J. W. Vieira, H. J. Khoury, F. R. A. Lima, E. C. M. Loureiro, V. J. M. Lima and G. Hoff "All about FAX: a Female Adult voXel Phantom for Monte Carlo Calculation in Radiation Protection Dosimetry", Phys. Med. Biol. **49**, 5203-5216 (2004)
[17] R. Kramer, H. J. Khoury, J. W. Vieira and V. J. M. Lima "MAX06 and FAX06: Update of two adult human phantoms for radiation protection dosimetry", Phys. Med. Biol. **51** 3331-3346 (2006)
[18] V. F. Cassola, V. J. de Melo Lima, R. Kramer and H. J. Khoury, "FASH and MASH: Female and Male Adult human phantoms based on polygon meSH surfaces. Part I: Development of the anatomy", Phys. Med. Biol. **55** 133-162 (2010)
[19] V. F.Cassola, R. Kramer, C. Brayner and H. J. Khoury, "Posture-specific phantoms representing female and male adults in Monte Carlo-based simulations for radiological protection", Phys. Med. Biol. **55** 4399-4430 (2010)
[20] V. F. Cassola, F. M. Milian, R. Kramer, C. A. B. de Oliveira Lima and H. J. Khoury, "Standing adult human phantoms based on 10^{th}, 50^{th} and 90^{th} mass and height percentiles of male and female Caucasian populations", Phys. Med. Biol. **56,** 3749-3772 (2011)
[21] P. Godin, "Record of individual growth: a guide to parents, physicians and teachers", Publications of the Training School at Vineland - New Jersey - Department of Research: Vineland (1916)
[22] L. Testut and A. Latarjet, "Tratado de anatomía humana", (Salvat, Barcelona, 1949)
[23] R.G. Snyder, L. W. Schneider, C. L. Owings, H. M. Reynolds, D. H. Golomb and M. A. Schork, "Anthropometry of Infants, Children, and Youths to Age 18 for Product Safety Design", U. S. Consumer Product Safety Commission: Bethesda, (1977)
[24] H. Gray, "Anatomia", 29. Edition, (Guanabara Koogan, Rio de Janeiro, 1977)
[25] J. MacGregor, "Introduction to the anatomy and physiology of children", (Rouledge, London, 2000)
[26] C. A. Chamley, P. Carson, D Randall and M. Sandwell,"Developmental Anatomy and Physiology of Children - A Practical Approach", (Elsevier, London, 2005)

[27] M. Schünke, E. Schulte and U. Schumacher," Prometheus, Atlas de anatomia: anatomia geral e aparelho locomotor", (Guanabara Koogan, Rio de Janeiro, 2006)
[28] M. Schünke, E. Schulte and U. Schumacher," Prometheus, Atlas de anatomia: pescoço e órgãos internos", (Guanabara Koogan, Rio de Janeiro, 2006)
[29] M. Schünke, E. Schulte and U. Schumacher," Prometheus, Atlas de anatomia: cabeça e neuroanatomia", (Guanabara Koogan, Rio de Janeiro, 2006)
[30] G. Wolff-Heidegger, "Atlas de anatomia humana", 6. Edition, 2nd volume, (Guanabara Koogan, Rio de Janeiro, 2006)
[31] K. L. Moore and A. F. Dalley, "Anatomia orientada para a clínica", 5. Edition, (Guanabara Koogan, Rio de Janeiro, 2007)
[32] R. A. Bergman, A. K. Afifi, J. J. Jew and P. C. Reimann, "Anatomy atlases", http://www.anatomyatlases.org, accessed January 1, 2010
[33] DISCIPLINA DE ANATOMIA DA FACULDADE DE MEDICINA DE PETRÓPOLIS. "Resumo da anatomia do recém nascido", http://www.compuland.com.br/anatomia/nascido.htm. Accessed January 18,2010.
[34] T. Rosendaal, Blender 2.49b, http://www.blender.org/ accessed September 1, 2009
[35] M. Bastioni, MakeHuman 0.9.1 RC1, http://www.makehuman.org, accessed March 24, 2009
[36] W. Rasband, ImageJ 1.43k, National Institute of Health, USA, http://rsbweb.nih.gov/ij, Accessed June 6, 2009
[37] J. W. Vieira, B. Stosic, F. R. A. Lima, R. Kramer, A. M. Dos Santos and V. J. M. Lima, "Um Software para Editar Fantomas de Voxels e Calcular Coeficientes de Conversão para a Proteção Radiológica", 1º Congresso Brasileiro de Proteção Radiológica, Rio de Janeiro, 02 a 05 de Novembro (2005)
[38] J. W. Vieira and F. R. A. Lima, "A Software to Digital Image Processing To Be Used in the Voxel Phantom Development, Cellular and Molecular Biology (Online), **55**, 16-22 (2009)
[39] V. F. Cassola, in-house code, private communication, August (2010)
[40] "Photon, Electron, Proton and Neutron Interaction Data for Body Tissues", ICRU Report 46, International Commission on Radiation Units and Measurements, Bethesda, Maryland, USA, (1992)
[41] R. Kramer, H. J. Khoury, J. W. Vieira and I. Kawrakow, "Skeletal dosimetry in the MAX06 and the FAX06 phantoms for external exposure to photons based on vertebral 3D-microCT images", Phys.Med.Biol. **51** 6265-6289 (2006)
[42] "Basic Anatomical and Physiological Data for use in Radiological Protection: The Skeleton", ICRP Publication 70, (Pergamon, Oxford, 1995)
[43] R. Kramer, V. F. Cassola, H. J. Khoury, J. W. Vieira, V. J. de Melo Lima and K. Robson Brown, " FASH and MASH: female and male adult human phantoms based on polygon mesh surfaces: II. Dosimetric calculations", Phys Med Biol **55** 163-189 (2010)
[44] "Adult Reference Computational Phantoms", ICRP Publication 110, (Pergamon, Oxford, 2009)
[45] A. Brito, "Blender 3D – guia de usuário", 3rd Edition, (Novatec, São Paulo, 2008)
[46] EGSnrc, version V4-2.3.1, available at http://irs.inms.nrc.ca/software/egsnrc/
[47] M. G. Stabin, R. B. Sparks and E. Crowe, "OLINDA/EXM: The Second-Generation Personal Computer Software for Internal Dose Assessment in Nuclear Medicine", J Nucl Med **46:** 1023-1027 (2005)
[48] T. J. Smith, A. W. Phipps, N. Petoussi-Henss and M. Zankl,"Impact on internal doses of photons SAFs derived with the GSF adult male voxel phantom", Health Phys. **80**(5), 477-485, 2001
[49] M. Zankl and A. Wittmann, "The adult male voxel model "Golem" segmented from whole-body CT patient data", Radiat Environ Biophys **40**, 153-162 (2001)
[50] D. Pafundi, D. Rajon, D. Jokisch, C. Lee and W.E. Bolch, "An image-based skeletal dosimetry model for the ICRP reference newborn – internal electron sources", Phys. Med. Biol. **55,** 1785-1814 (2010)
[51] R. Kramer, R.B. Richardson, V.F. Cassola, J.W. Vieira, H.J. Khoury, C.A.B. de Oliveira Lira and K. Robson Brown, "Electron absorbed fractions of energy and S-Values in an adult human skeleton based on μCT images of trabecular bone", Phys. Med. Biol. **56,** 1803-1836 (2011)

Table 1. Tissue masses, densities and calculated volumes for the 5- and 10-year-old skeletons. Data taken from ICRP89 [10] and ICRU46 [40].

Skeletal region	5 years mass (g)	5 years density (g cm^{-3})	5 years volume (cm^3)	10 years mass (g)	10 years density (g cm^{-3})	10 years volume (cm^3)
Bone, cortical	1010	1.70	594.1	1840	1.75	1051.4
Bone, trabecular	250	1.70	147.1	460	1.75	262.9
Bone, total	1260	1.70	741.2	2300	1.75	1314.3
Marrow, active (red)	340	1.03	330.1	630	1.03	611.7
Marrow, inactive (yellow)	160	0.98	163.3	630	0.98	642.9
Cartilage	600	1.10	545.5	820	1.10	745.5
Teeth	15	2.75	5.5	30	2.75	10.9
Miscellaneous	55	1.03	53.4	90	1.03	87.4
Total skeleton	2430	1.32	1839.0	4500	1.32	3412.7

Table 2. Bone mass fractions, RBM mass fractions and cellularity factors for the 5- and 10-year-old skeletons. Mass ratios between cortical and trabecular bone are for the adult skeleton. The quantities were taken or calculated from data found in ICRP89 [10] and ICRP70 [42].

Skeletal region	5 years Bone mass fraction	5 years RBM mass fraction	5 years Cellularity factor	10 years Bone mass fraction	10 years RBM mass fraction	10 years Cellularity factor	Adult Mass ratio of bone cortical / trabecular
Wrist and hand bones	0.017	0.009	0.20	0.020	0.000	0.00	95 / 5
Radii and Ulnae	0.034	0.020	0.57	0.041	0.011	0.23	85.5 / 14.5
Humeri, upper half	0.022	0.024	0.77	0.026	0.025	0.60	80 / 20
Humeri, lower half	0.022	0.022	0.71	0.026	0.016	0.39	80 / 20
Ribs	0.075	0.088	0.85	0.069	0.109	0.80	94 / 6
Sternum	0.005	0.017	0.85	0.006	0.021	0.80	94 / 6
Scapulae	0.022	0.027	0.80	0.024	0.029	0.65	94 / 6
Clavicles	0.007	0.009	0.79	0.008	0.009	0.63	94 / 6
Cervical vertebrae	0.020	0.022	0.85	0.018	0.027	0.80	25 / 75
Thoracic vertebrae	0.049	0.089	0.85	0.045	0.109	0.80	25 / 75
Lumbar vertebrae	0.042	0.068	0.85	0.038	0.084	0.80	34 / 66
Sacrum	0.024	0.055	0.85	0.023	0.067	0.80	75 / 25
Cranium	0.371	0.159	0.80	0.285	0.116	0.65	95 / 5
Mandible	0.037	0.016	0.80	0.029	0.011	0.65	95 / 5
Pelvis	0.047	0.131	0.79	0.063	0.156	0.72	90 / 10
Femora, upper half	0.051	0.068	0.77	0.069	0.094	0.60	67 / 33
Femora, lower half	0.051	0.063	0.71	0.069	0.061	0.39	67 / 33
Tibiae,fibulae, patellae	0.075	0.090	0.57	0.101	0.055	0.23	75 / 25
Ankle and foot bones	0.030	0.025	0.20	0.041	0.000	0.00	95 / 5

Table 3. Trabecular bone volume fractions for adult and pediatric skeletons. The adult TBVFs are from the original μCT images used in the paper of Kramer et al [43], while the pediatric TBVFs have been derived from the adult TBVFs.

Bone site	Trabecular bone volume fraction (%)		
	Adult	5-year	10-year
Frontal bone	51.6	75.1	68.1
Vertebra L1	11.3	20.7	17.6
Sternum	11.4	20.9	17.3
Iliac crest	21.2	20.7	17.6
Femur	15.2	26.3	26.3

Table 4. Some important properties of the voxelized pediatric phantoms M05, F05, M10 and F10

Properties of the voxelized phantoms	5-year-old	10-year-old
Organs and tissues segmented (male/female)	142/143	142/143
Voxel size (μm x μm x μm)	700 x 700 x 700	700 x 700 x 700
Number of columns	568	706
Number of lines	286	314
Number of slices	1557	1971
Standing height (cm)	108.99	137.97
Total body mass (kg) (male/female)	19.13/19.12	32.34/32.30

Table 5. Bone-specific skeletal tissue volumes for the 5-year-old skeleton calculated from the data shown in tables 1 and 2

5 year Skeletal region	Cortical bone (cm^3)	Spongiosa (cm^3)	YBM med (cm^3)	RBM med (cm^3)	Cart/misc (cm^3)	Total (cm^3)
Wrist and hand bones	12.0	15.5			10.2	37.6
Radii and Ulnae	21.5	15.2	1.8	2.4	20.4	58.9
Humeri, upper half	13.0	13.5	0.6	2.1	13.2	40.4
Humeri, lower half	13.0	13.5	0.8	1.9	13.2	40.5
Ribs	52.3	37.5			44.9	134.7
Sternum	3.5	6.8			3.0	13.3
Scapulae	15.3	12.1			13.2	40.6
Clavicles	4.9	4.1			4.2	13.1
Cervical vertebrae	3.7	19.7			12.0	35.3
Thoracic vertebrae	9.1	61.8			29.3	100.2
Lumbar vertebrae	10.6	47.0			25.1	82.7
Sacrum	13.3	25.8			14.4	53.5
Cranium	261.2	79.4			221.5	562.1
Mandible	26.1	8.0			22.2	56.2
Pelvis	31.4	58.2			28.1	117.7
Femora, upper half	25.3	41.6	0.8	2.7	30.5	98.3
Femora, lower half	25.3	41.8	1.0	2.5	30.5	98.6
Tibiae, fibulae, patellae	41.7	66.0	2.2	2.9	44.9	154.8
Ankle and foot bones	21.1	42.4			18.0	81.5
Total	604.4	609.8	7.2	14.5	598.7	1834.7
ICRP89 (no teeth)						1833.5

Table 6. Bone-specific skeletal tissue volumes for the 10-year-old skeleton calculated from the data shown in tables 1 and 2.

10 year Skeletal region	Cortical bone (cm^3)	Spongiosa (cm^3)	YBM med (cm^3)	RBM med (cm^3)	Cart/misc (cm^3)	Total (cm^3)
Wrist and hand bones	25.0	13.0			16.7	54.6
Radii and Ulnae	46.1	37.1	18.5	5.5	34.1	135.8
Humeri, upper half	27.3	32.3	6.1	9.1	21.6	87.4
Humeri, lower half	27.3	31.9	9.3	5.9	21.6	90.2
Ribs	85.2	88.8			57.4	231.5
Sternum	7.4	16.5			5.0	28.9
Scapulae	29.7	29.2			20.0	78.8
Clavicles	9.9	9.4			6.7	25.9
Cervical vertebrae	5.9	38.4			15.0	59.3
Thoracic vertebrae	14.8	127.7			37.5	180.0
Lumbar vertebrae	17.0	97.2			31.6	145.8
Sacrum	22.7	58.8			19.1	100.6
Cranium	355.8	127.9			236.5	720.2
Mandible	36.2	12.3			24.1	72.6
Pelvis	74.5	140.8			52.5	267.8
Femora, upper half	60.8	125.8	16.2	24.2	57.4	260.1
Femora, lower half	60.8	125.6	24.6	15.8	57.4	268.4
Tibiae, fibulae, patellae	99.6	179.5	45.5	13.6	84.1	408.6
Ankle and foot bones	51.2	26.7			34.1	112.0
Total	1057.1	1318.7	120.1	74.2	832.6	3402.7
ICRP89 (no teeth)						3401.8

Table 7. Organ and tissue masses for the 5- and 10-year-old ICRP reference children and for the voxelized pediatric phantoms M05, F05, M10 and F10

	5-year-old male		5-year-old female		10-year-old male		10-year-old female	
	ICRP89	M05	ICRP89	F05	ICRP89	M10	ICRP89	F10
ORGAN / TISSUE	[g]	[g]	[g]	[g]	[g]	[g]	[g]	[g]
Adrenals	5.0	5.0	5.0	5.0	7.0	7.0	7.0	7.0
Salivary Glands	34.0	34.0	34.0	34.0	44.0	44.0	44.0	44.0
Esophagus	10.0	10.0	10.0	10.0	18.0	18.0	18.0	18.0
Stomach wall	50.0	50.0	50.0	50.0	85.0	85.0	85.0	85.0
Small Intestine wall	220.0	220.0	220.0	220.0	370.0	370.0	370.0	370.0
Colon wall	120.0	120.0	120.0	120.0	210.0	210.0	210.0	210.0
Liver	570.0	570.0	570.0	570.0	830.0	830.0	830.0	830.0
Gallbladder wall	2.6	2.6	2.6	2.6	4.4	4.4	4.4	4.4
Pancreas	35.0	35.0	35.0	35.0	60.0	60.0	60.0	60.0
Brain	1310.0	1310.0	1180.0	1180.0	1400.0	1400.0	1220.0	1220.0
Heart wall	85.0	85.0	85.0	85.0	140.0	140.0	140.0	140.0
Adipose	5000.0	5000.0	5000.0	5000.0	7500.0	7500.0	7500.0	7500.0
Skin	570.0	570.0	570.0	570.0	820.0	820.0	820.0	820.0
Muscle	5600.0	5600.0	5600.0	5600.0	11000.0	11000.0	11000.0	11000.0
Lungs	300.0	300.0	300.0	300.0	500.0	500.0	500.0	500.0
Skeleton	2430.0	2439.3	2430.0	2439.3	4500.0	4537.9	4500.0	4537.9
Spleen	50.0	50.0	50.0	50.0	80.0	80.0	80.0	80.0
Thymus	30.0	30.0	30.0	30.0	40.0	40.0	35.0	35.0
Thyroid	3.4	3.4	3.4	3.4	7.9	7.9	7.9	7.9
Kidneys	110.0	110.0	110.0	110.0	180.0	180.0	180.0	180.0
Bladder wall	16.0	16.0	16.0	16.0	25.0	25.0	25.0	25.0
Testes	1.7	1.7			2.0	2.0		
Prostate	1.2	1.2			1.6	1.6		
Ovaries			2.0	2.0			3.5	3.5
Uterus			3.0	3.0			4.0	4.0
Fallopian tubes			0.35	0.35			0.5	0.5
Tongue	19.0	19.0	19.0	19.0	32.0	32.0	32.0	32.0
Larynx	7.0	7.0	7.0	7.0	12.0	12.0	12.0	12.0
Pharynx		11.3		11.3		11.6		11.6
Nasal passage		27.2		27.2		43.3		43.3
Paranasal sinus, ears		12.4		12.4		15.1		15.1
Mouth cavity		46.6		46.6		41.7		41.7
Bronchi		1.8		1.8		3.4		3.4
GI content	300.0	300.0	300.0	300.0	420.0	420.0	420.0	420.0
Gall bladder cont.	15.0	15.0	15.0	15.0	26.0	26.0	26.0	26.0
Trachea	2.5	2.5	2.5	2.5	4.5	4.5	4.5	4.5
Tonsils	2.0	2.0	2.0	2.0	3.0	3.0	3.0	3.0
Ureter	4.2	4.2	4.2	4.2	7.0	7.0	7.0	7.0
Urethra	2.6	2.6	0.78	0.78	4.4	4.4	1.3	1.3
Epididymes	0.45	0.45	0.45	0.45	0.60	0.60	0.60	0.60
Pituary Gland	0.25	0.25	0.25	0.25	0.35	0.35	0.35	0.35
Eyes	11.0	11.0	11.0	11.0	12.0	12.0	12.0	12.0
Blood*	1500.0	262.9	1500.0	262.9	2500.0	520.2	2500.0	520.2
Spinal chord		12.4		12.4		16.4		16.4
Connective Tissue	700.0	567.7	700.0	567.7	1100.0	967.7	1100.0	967.7
Lymphatic Nodes	60.0	60.0	60.0	60.0	180.0	180.0	180.0	180.0
Other tissues**		1200.3		1323.3		2159.6		2302.3
Total mass	19177.9	19129.8	19048.5	19123.4	32126.8	32343.6	31943.1	32302.6

* without lungs ** includes soft tissue, blood, etc.

Figure 1. Interface of the MakeHuman [35] software showing the parameter controls for AGE/SEX, BODY MASS, BREAST and BODY SHAPE as well as the body surface for the 10-year-old child modeled for this study.

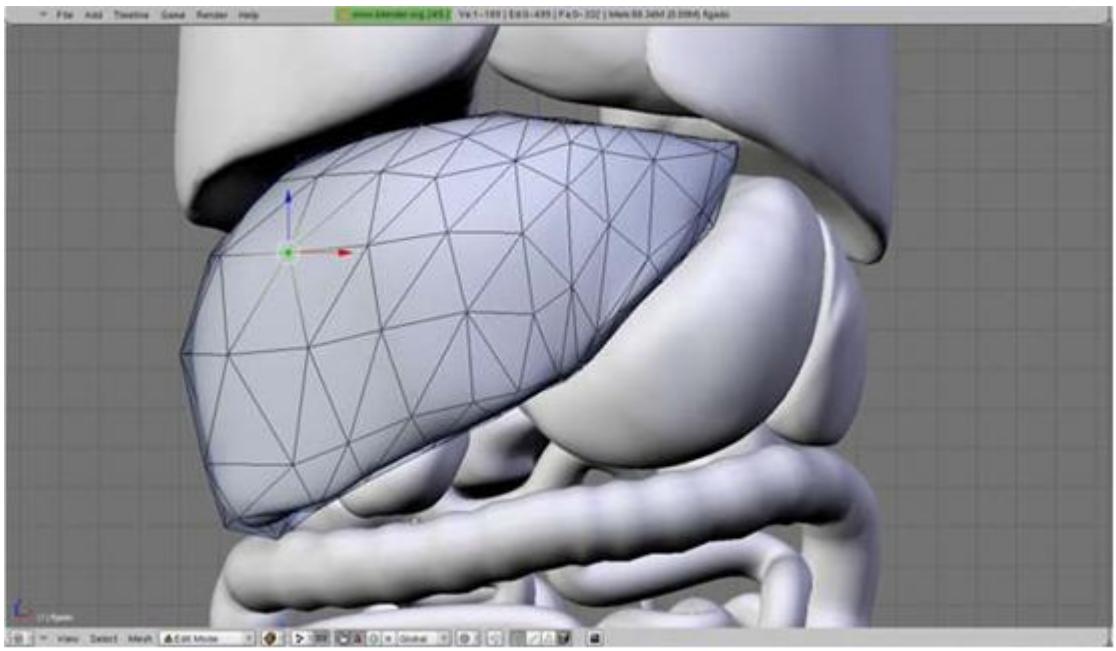

Figure 2. Interface of the Blender [34] software showing abdominal organs and highlighting a control point on the polygon mesh surface representing the liver.

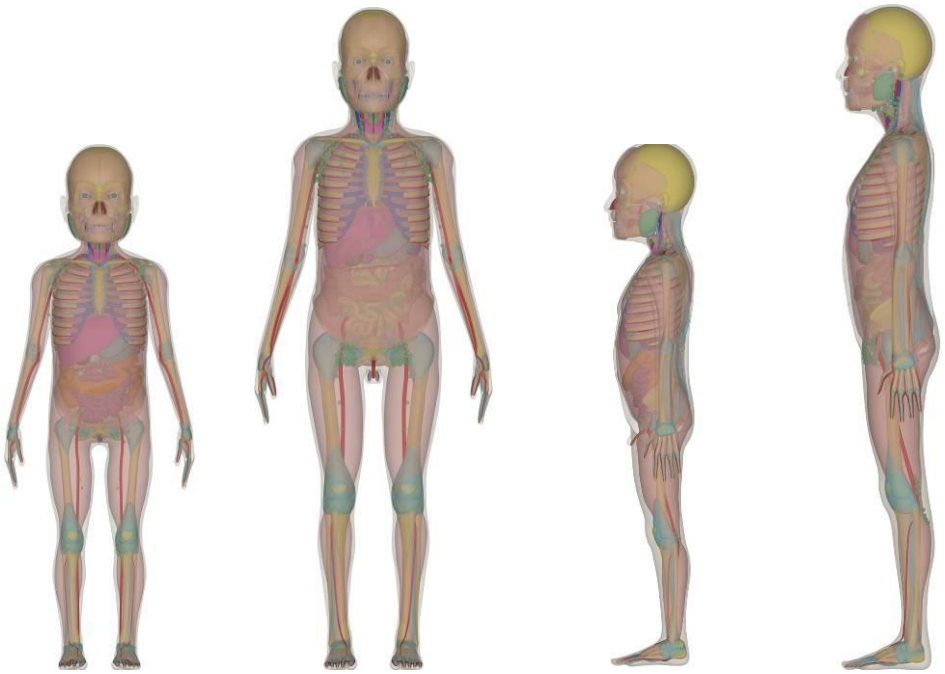

Figure 3. Anterior (left) and lateral (right) views of the male and female 5- and 10-year-old pediatric mesh phantoms, called M05, F05 and M10, F10, showing body contours, superficial organs, skeletons, internal organs and blood vessels.

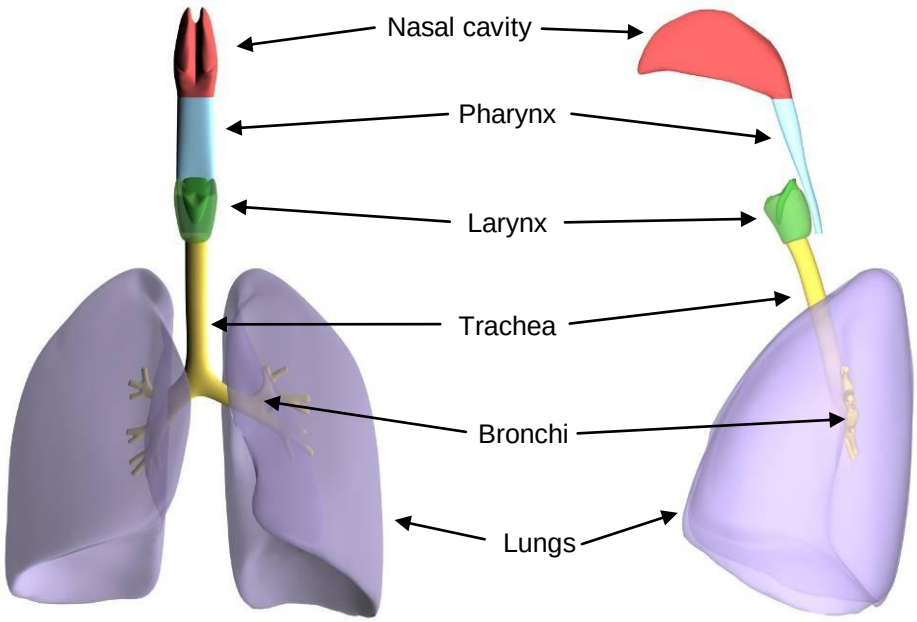

Figure 4. Anterior (left) and lateral (right) views of the organs and tissues of the respiratory system for the 10-year-old mesh phantoms F10 and M10

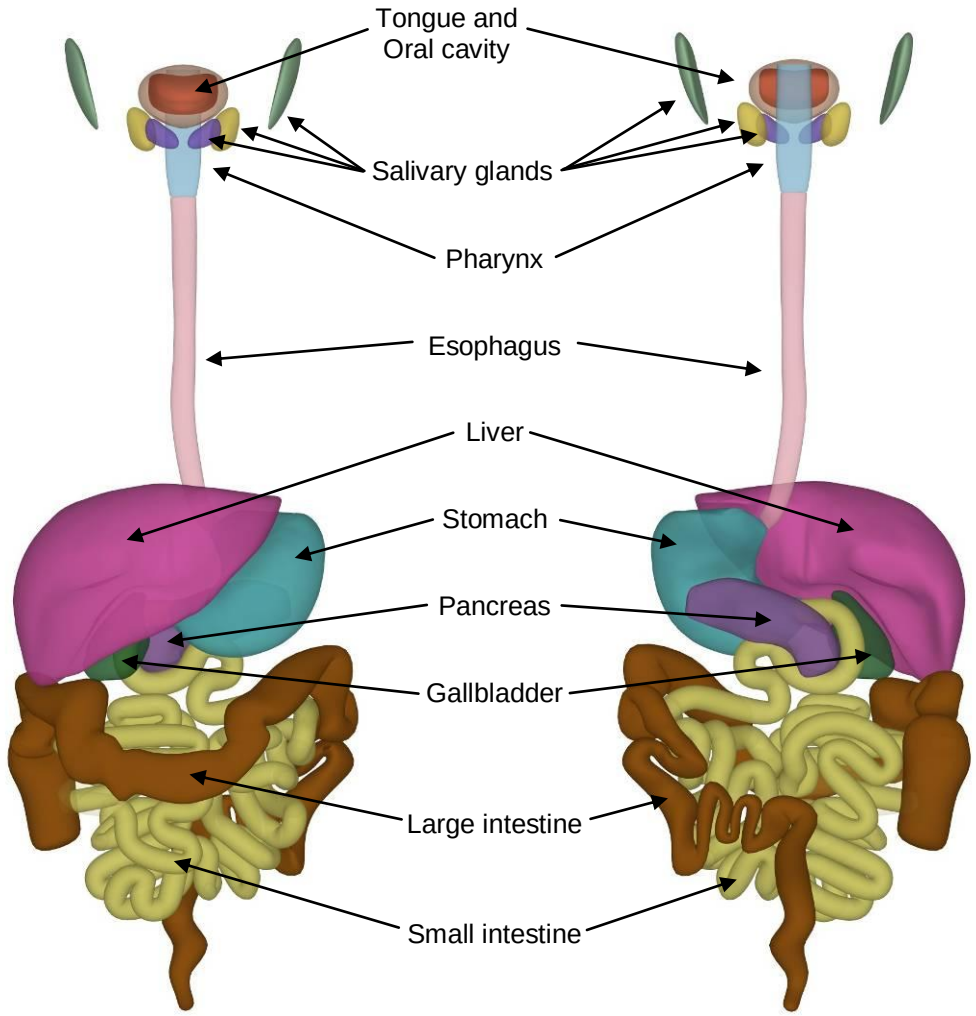

Figure 5. Anterior (left) and posterior (right) views of the organs of the digestive system for the 10-year-old mesh phantoms F10 and M10.

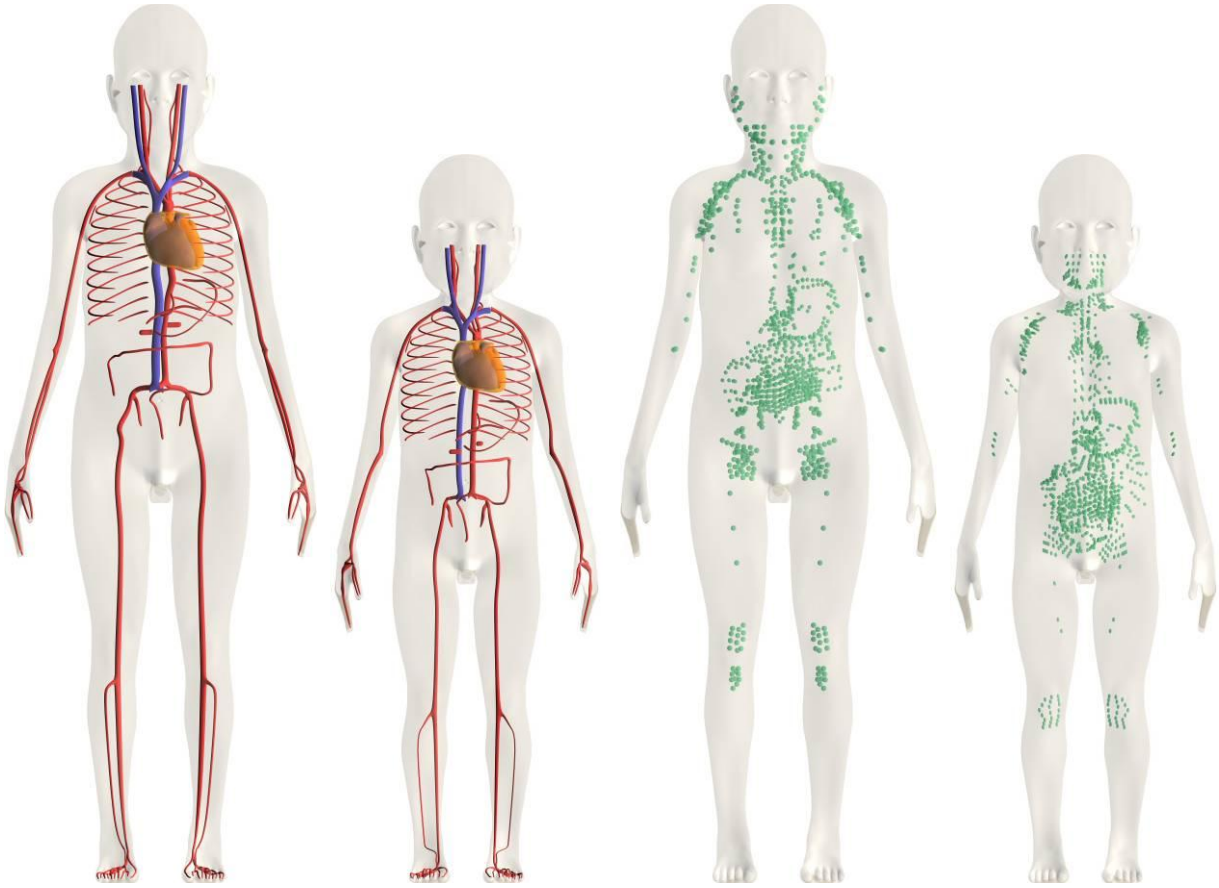

Figure 6. Anterior views of the circulatory (left) and the lymphatic (right) systems for the 5- and 10-year-old mesh phantoms F05, M05, F10 and M10.

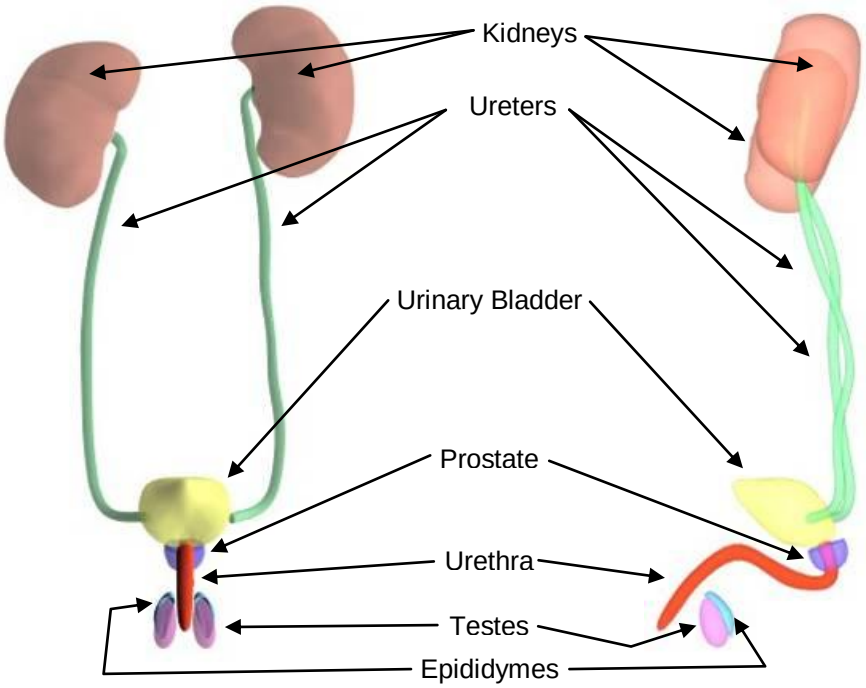

Figure 7. Anterior (left) and lateral (right) views of the organs of the urogenital system for the male 5-year-old mesh phantom M05

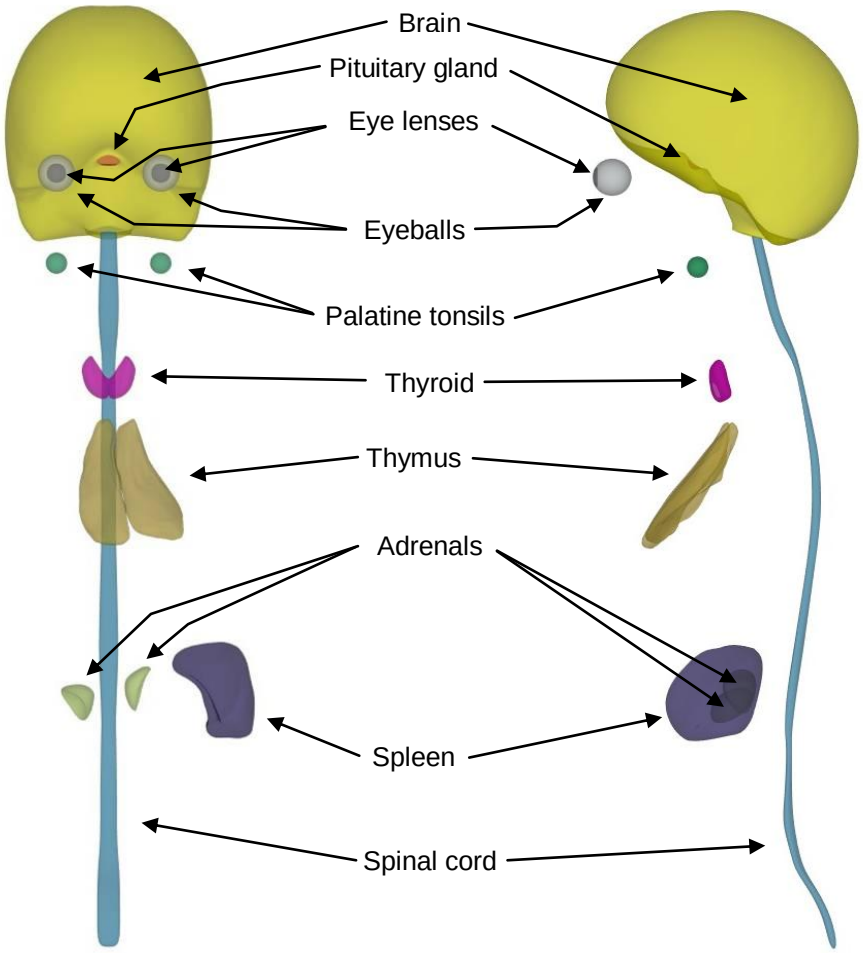

Figure 8. Anterior (left) and lateral (right) views of additional organs for the 5-year-old mesh phantoms F05 and M05.

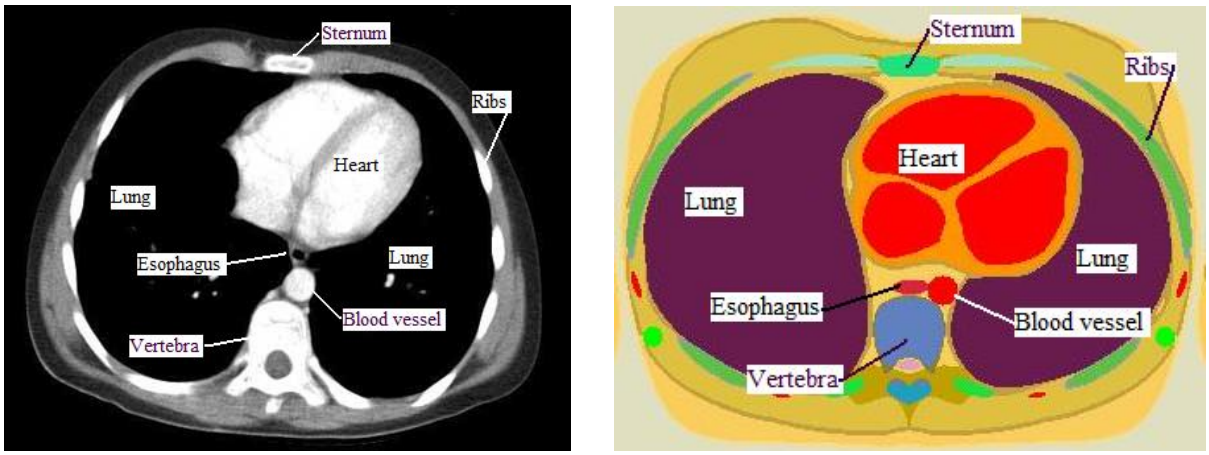

(a) (b)

Figure 9a, b. Chest CT image of a 9-year-old boy in supine posture (a) and the corresponding transversal slice of the standing M10 phantom (b).

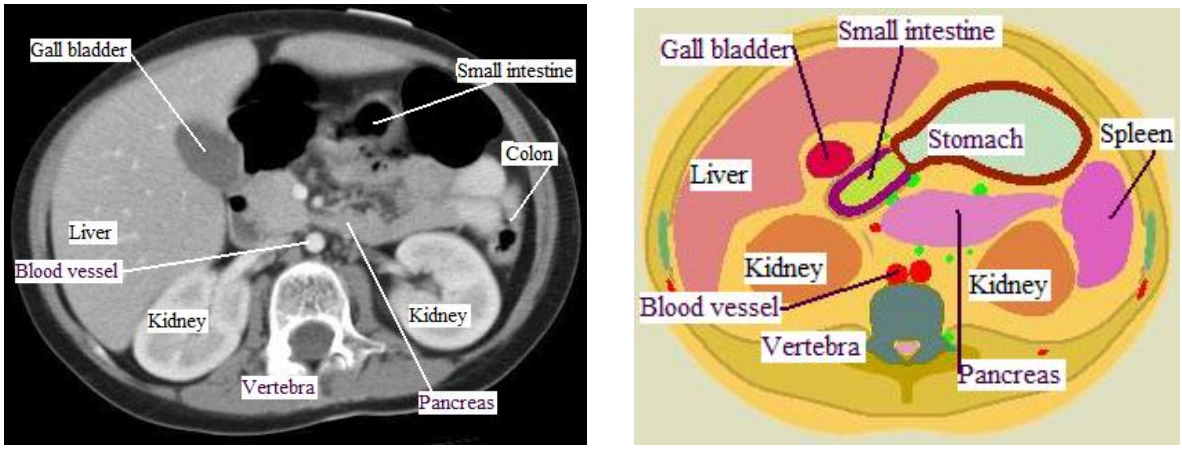

(a) (b)

Figure 10a, b. Abdominal CT image of a 9-year-old boy in supine posture (a) and the corresponding transversal slice of the standing M10 phantom (b).

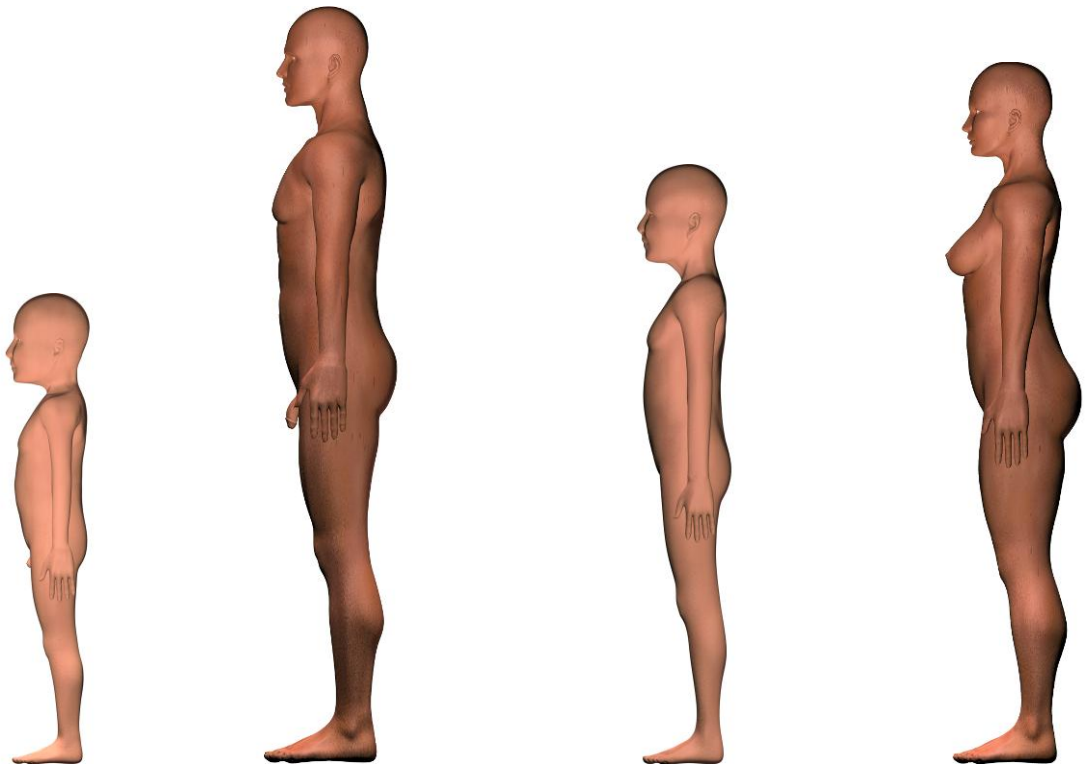

M05 MASH3 F10 FASH3

Figure 11. Lateral views of the pediatric mesh phantoms M05 and F10 and of the adults mesh phantoms MASH3 and FASH3

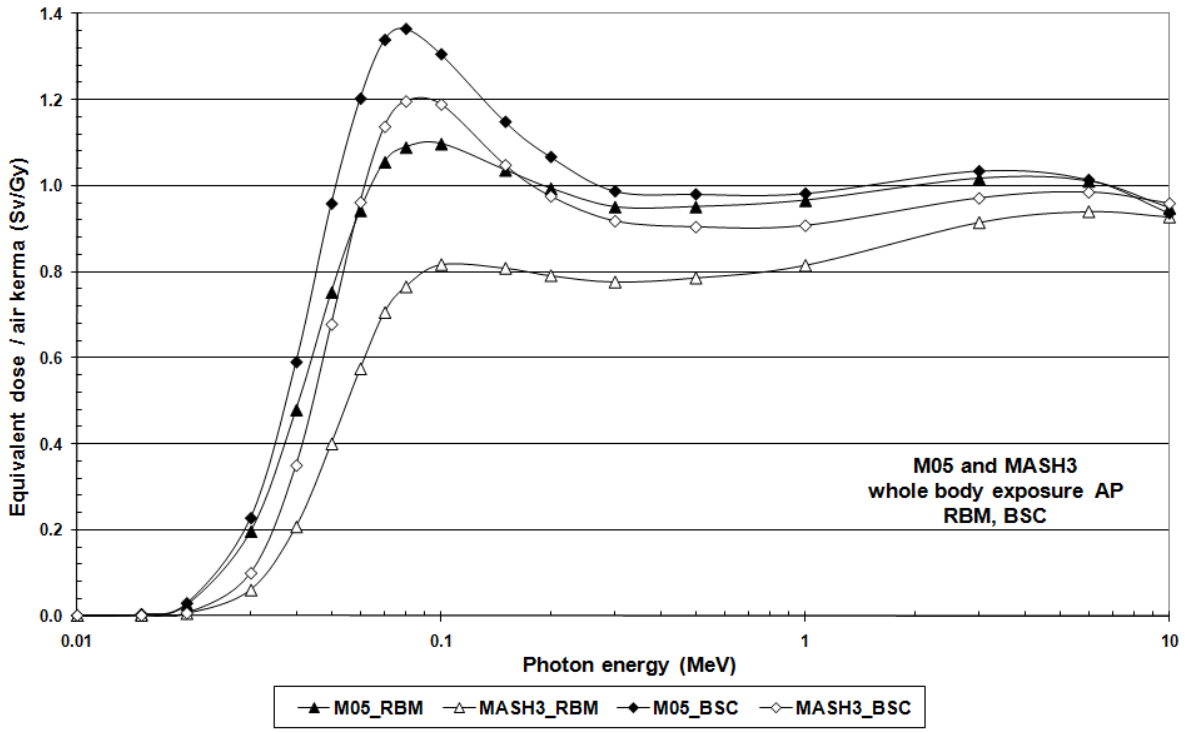

Figure 12. Conversion coefficients between RBM and BSC equivalent dose and air kerma free-in-air for the M05 and the MASH3 phantoms for whole body exposure AP with monoenergetic photons between 10 keV and 10 MeV.

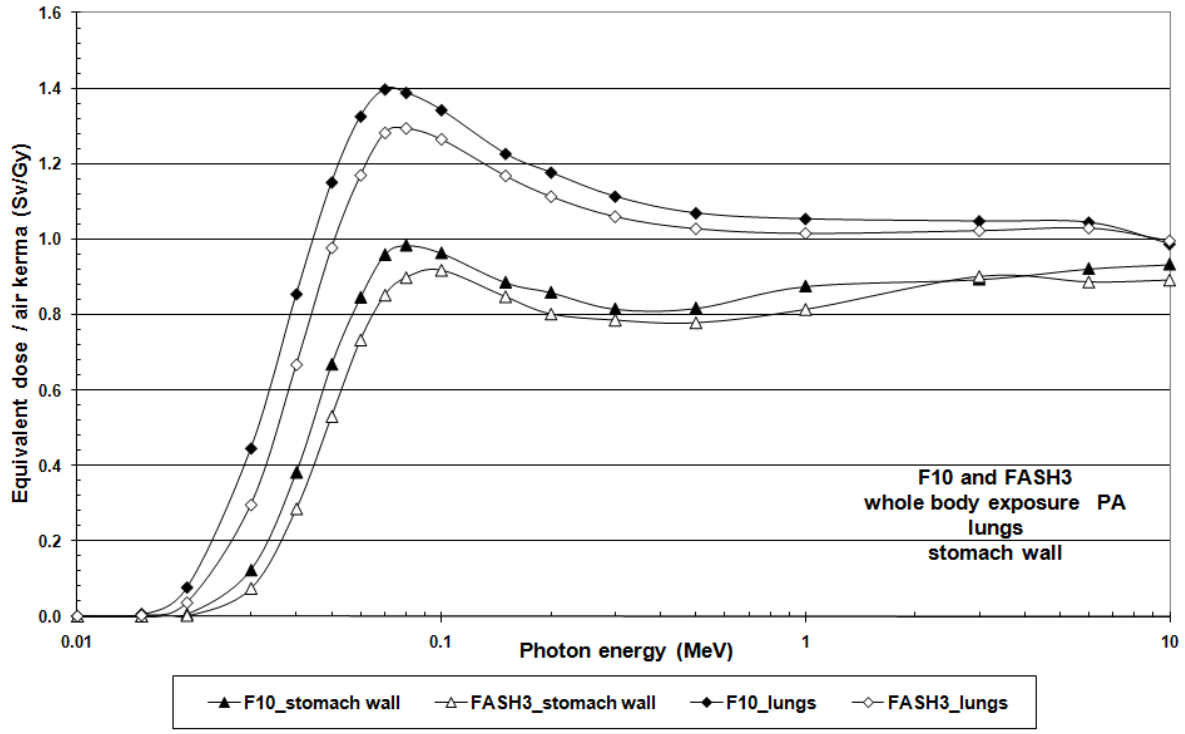

Figure 13. Conversion coefficients between lungs and stomach wall equivalent dose and air kerma free-in-air for the F10 and the FASH3 phantoms for whole body exposure AP with monoenergetic photons between 10 keV and 10 MeV.

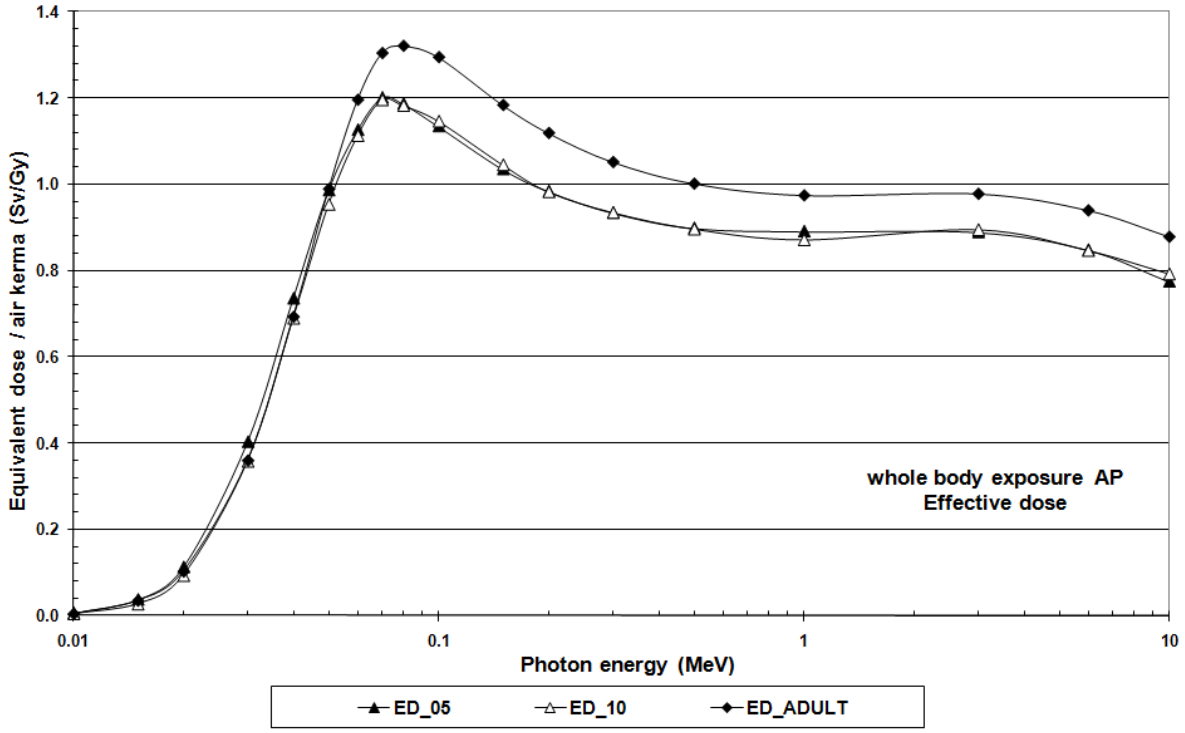

Figure 14. Conversion coefficients between effective dose (ED) and air kerma free-in-air for the pediatric and the adult phantoms for whole body exposure AP with monoenergetic photons between 10 keV and 10 MeV.

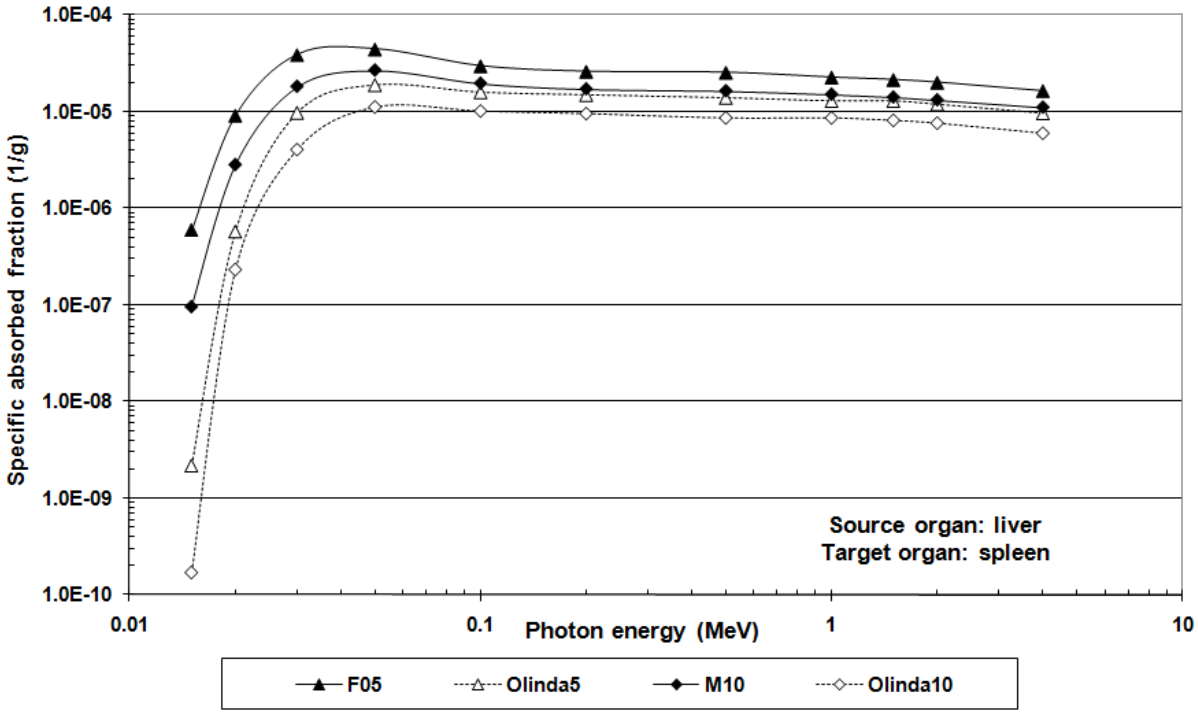

Figure 15. Specific absorbed fractions of energy in the spleen of the F05, M10, and the 5- and 10-year-old MIRD5 phantoms when the liver is the source organ. The MIRD5 data have been calculated with the OLINDA software [47].